Faraday Discussions

RSC Publishing

Cite this: *Faraday Discuss.*, 2013, **166**, 151

PAPER

View Article Online
View Journal | View Issue

Polymorphism in bovine serum albumin fibrils: morphology and statistical analysis

Ivan Usov, Jozef Adamcik and Raffaele Mezzenga*

Received 10th May 2013, Accepted 5th June 2013
DOI: 10.1039/c3fd00083d

We investigate the self-assembly process of the globular protein bovine serum albumin (BSA) into fibrillar structures upon incubating the protein solution at high temperature (90 °C) and in an acidic environment (pH 2) for several days. The investigation is performed by atomic force microscopy (AFM) on the self-assembled fibrillar structures, adsorbed on mica substrates from a solution at different fibrillation time snapshots. A rigorous study of structural morphology reveals a sophisticated hierarchy of the BSA fibrils, where two major classes can be identified: flexible and rigid fibrils, with an order of magnitude of difference in their stiffness. Furthermore, each main class can be divided into two subclasses of thin and thick fibrils according to their average height. It is also shown that all types of flexible ribbon-like fibrils at some stage can wrap and close into nanotubes, that is into a rigid class of fibril. A precise statistical analysis of all the subclasses identified is developed throughout the manuscript. The determination of height and contour length distributions, persistence lengths, and other topological characteristics is carried out by processing the coordinates of BSA fibrils acquired from AFM imaging using in-house developed software. The resulting statistical analysis allows better understanding the fibrillation process and the structural properties of the BSA fibrils.

1. Introduction

The folding of proteins into perfectly-defined three-dimensional secondary and tertiary structures is a very important process on which depends the correct biological function of the proteins. However, this folding process can fail causing the formation of disordered or highly ordered aggregate structures.[1–4] The occurrence of protein aggregation is an unavoidable part of everyday life and *in vivo* is related to diseases such as Parkinson's, Alzheimer's, Creutzfeldt-Jakob's, type II diabetes, and bovine spongiform encephalopathy, where the proteins or peptides self-assemble into highly ordered fibrillar structures, referred to as amyloid fibrils.[5–9] Protein aggregation can also be controlled *in vitro* such as in the case of food processing, since many globular proteins, major components of food

ETH Zurich, Food & Soft Materials Science, Institute of Food, Nutrition & Health, Schmelzbergstrasse 9, LFO E23, 8092 Zurich, Switzerland. E-mail: raffaele.mezzenga@hest.ethz.ch

products, also have a tendency to self-assemble into amyloid fibrils.[10–13] Thus, the understanding of the fibrillation mechanisms can serve both the medical field, when dealing with neurodegenerative diseases, as well as food processing, to engineer and improve the possible use of these structures as texture builders, foaming or gelling agents.[14,15] In addition, amyloid fibrils possess unique mechanical properties including high elasticity and strength.[16] Thus, they are also suitable candidates for nanotechnology and biomaterials applications.[17–21]

A globular protein in its native form has a stable conformation, hence the transformation to the fibrillar structure requires an unfolding process,[3,22] which *in vitro* is very often performed by heat treatment of a solution above the protein denaturation temperature. Furthermore, other factors such as ionic strength, pH, enzymatic treatment or presence of denaturation surfactants can have a strong influence on the protein unfolding process.

The field of globular protein fibrillation has undergone rapid development in recent years,[23] with an accurate description of the structure and properties being provided both at the single molecule and collective molecules length scales.[24–26] The formation of amyloid-like fibrils has been reported for a broad range of globular proteins such as ovalbumin,[12,27,28] β-lactoglobulin,[12,29–36] lysozyme[24,35,37–39] and α-lactalbumin.[29,36,40] However, the conditions for the fibrillation processes for all the proteins mentioned typically vary to a great extend; for example, incubation temperatures are in the range of 50–90 °C, and both low or high ionic strengths are used together with a wide range of pHs. We have previously reported the formation of amyloid-like fibrils for three types of globular proteins: β-lactoglobulin,[35] lysozyme[35] and ovalbumin,[27] under particular incubation conditions, such as pH 2 and elevated temperature (90 °C). In all cases the formation of long semiflexible fibrils was observed. In addition, in the case of β-lactoglobulin and lysozyme at longer incubation times (several days) the formation of giant helical multi-stranded ribbons consisting of up to 17 protofilaments was shown.[35] Other authors have reported that the globular protein bovine serum albumin (BSA), with an isoelectric point of 4.7[41] can self-assembly *in vitro* into amyloid-like fibrillar structures under a variety of conditions, including relatively high temperatures between 60–80 °C, the presence of salt during incubation and different pHs.[42–54]

Atomic force microscopy (AFM) is a powerful technique to study the kinetics of the fibrillation process, as well as some of the properties of amyloid fibrils.[55] Morphological parameters such as contour length, height, persistence length or pitch can be easily extracted from AFM images. The statistical analysis of these parameters can yield a precise description of the structural packing model of individual protofilaments within the same fibril, as in the case of β-lactoglobulin,[56] and important topological details of amyloid fibrils during their growth from a single protofilament to mature fibrils.[31] Beyond structural characterization, the analysis of AFM images is also used to estimate the mechanical properties of amyloid fibrils.[57,58] In addition, AFM working in spectroscopy mode enables the Young's modulus of amyloid fibrils to be obtained by the quantification of the tip–surface interaction forces.[55,59] Recently, a new AFM technique called peak force quantitative nanomechanical AFM (PF-QNM) was developed to extract the mechanical properties from a wide range of samples including amyloid fibrils.[60–62]

Since BSA has already been reported to self-assemble into fibrils under a broad range of conditions, we set out to provide a detailed characterization of the

fibrillation process occurring at pH 2 and 90 °C. We then perform an accurate statistical analysis of the topological parameters emerging from AFM analysis to draw conclusions on the fibrillation process and fibrils structure.

2. Methods

Preparation of the BSA fibrils

BSA powder obtained from Sigma (A7030, lyophilized powder ≥98%) was first dialyzed in order to remove salt ions and fatty acid impurities. A vessel containing 1.5 g of protein dissolved in 23.5 ml of pH 2 Milli-Q water (6% w/w of the final protein concentration) was incubated in an oil bath at 90 °C for up to 145 hours. Mild stirring was applied during the whole incubation period. To follow the fibrillation kinetics without a significant change of the solution volume and hence stirring conditions, small aliquots (0.7 ml) were taken at different incubation times (0.5, 1, 2, 3, 4, 5, 6, 20, 40, 70, 100, and 145 hours) and immediately placed in a cooling bath in order to quench the high temperature incubation process at a fixed time.

AFM measurements

The samples for AFM measurements were prepared in the following way: solutions of 6% w/w taken at different incubation times were diluted to a final concentration of 0.1% w/w with pH 2 Milli-Q water. Then 20 μl aliquots were deposited on freshly cleaved mica discs for 2 minutes, rinsed with Milli-Q water and gently dried with an air flow. AFM measurements were carried out with a MultiMode VIII Scanning Probe Microscope (Bruker, USA) operated in tapping mode under ambient conditions and with cantilevers having a nominal vibrating frequency of 150 kHz. The images were flattened using the Nanoscope 8.1 software, and no further image processing was carried out.

Tracking of the fibrils

Coordinate acquisition of the fibrils and their statistical analysis were performed by an in-house developed software written in MATLAB.[63] A slightly modified Open Active Contours algorithm[64,65] together with an A* pathfinding algorithm[66] were used to track the fibrils. AFM images of the sample after 40 hours of incubation were used to obtain coordinates of the flexible fibrils, while rigid fibrils were tracked on images of the 100 hours sample. In total 1429 flexible (1133 thick and 296 thin) and 807 rigid (680 thick and 127 thin) objects were traced. All statistical results were extracted from high-resolution AFM images (15 × 15 μm, 5120 × 5120 pixels). In addition, 1808 rigid fibrils imaged with a large AFM scanner (100 × 100 μm, 5120 × 5120 pixels) were used for persistence length and length distribution determination. This was done to increase the number of fibrils that do not cross the image edge and hence, preventing contour length estimation errors.

3. Results and discussion

BSA was dissolved in pH 2 water at a final concentration of 6% w/w and was then incubated at 90 °C according to the well-established protocols for the formation of β-lactoglobulin,[30,35] lysozyme,[35] and ovalbumin amyloid fibrils.[27] At fixed times of

incubation (0.5, 1, 2, 3, 4, 5, 6, 20, 40, 70, 100, and 145 hours) samples were taken to follow the fibrillation process by AFM.

Fig. 1 illustrates AFM images of the fibrillar structures formed at different incubation times. It took roughly 6 hours for the first flexible fibrils to appear [Fig. 1(a)]. Images of samples taken before that time display only tiny point-like segments – in the case of 5 hours incubation period – or reveal bare mica during the first hours of incubation (data not shown). For up to 40 hours the contour length and the density of the flexible fibrils increase monotonically, as can be seen in Fig. 1(b) and Fig. 1(c). These flexible fibrils possess an analogous shape to the fibrils reported previously, assembled at around 60 °C, pH 2, in the presence of salt, and upon incubation for 40 hours.[12,25,28] In all the above-mentioned studies rigid fibrils have never been detected. However, we could resolve a new class of rigid fibrils that originates between 40 and 70 hours of incubation time and, from this time onwards, coexists with the flexible fibrils [Fig. 1(d)]. The coexistence of flexible and rigid fibrils has been reported so far for ovalbumin fibrillation[27] and in the case of β-lactoglobulin fibrils incubated in an ethanol–water mixture.[67]

With the incubation time progressing, the contour length of the fibrils consequently increases, and upon stirring the fibrils start to entangle and aggregate. This causes a depletion of the amount adsorbed uniformly on the substrate [Fig. 1(d–f)] and the formation of large aggregates in the solution after 100 and 145 hours, as displayed in Fig. 2. The presence of aggregated stacks simultaneously leads to the solution becoming more viscous and turbid, and becoming brownish in colour (data not shown).

The results from previous studies on BSA fibrillation[28] indicate that the aggregation process in the 5% w/w BSA solution at pH 2, 0.2 M salt concentration, 60 °C and 1 hour of incubation is reversible within minutes after dilution by a factor of 100 and there is a critical concentration necessary for the self-assembly. In order to verify the stability of the BSA fibrils in our experiments after a drop in concentration from 6% w/w to 0.1% w/w (by a factor of 60), one diluted sample (at 100 hours of incubation) was kept at 4 °C for 7 days, and then analysed by AFM. The morphology imaged for this sample is similar to that in Fig. 1(e), with all

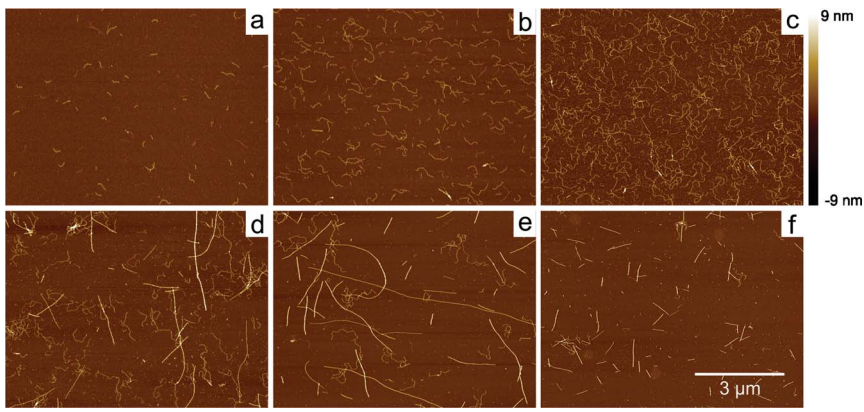

Fig. 1 AFM snapshots of the 6% w/w BSA fibrillation at 90 °C after (a) 6 hours, (b) 20 hours, (c) 40 hours, (d) 70 hours, (e) 100 hours, and (f) 145 hours of incubation. Concentration upon deposition is 0.1% w/w in all cases. Scale bars apply to all images.

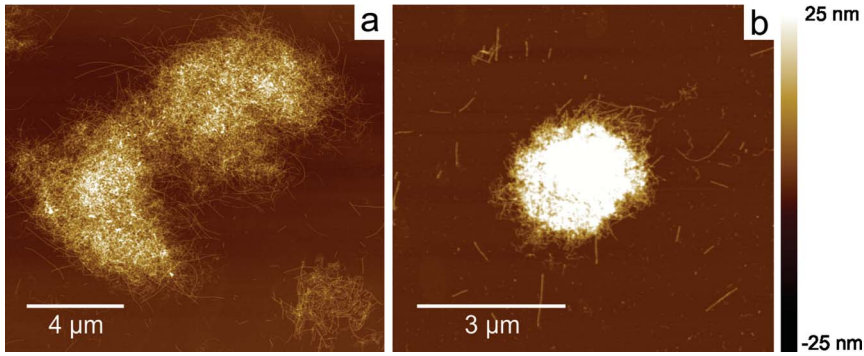

Fig. 2 AFM images of the large BSA fibril aggregates after (a) 100 hours, and (b) 145 hours of incubation. Colour scale bar applies to both images.

classes of fibrils still present on the mica and analogous length distributions (data not shown), suggesting an irreversible process.

Up to now we have referred to flexible and rigid groups of fibrils as the two major classes. However, further analysis of the height values reveals a more intricate hierarchy of morphologies. Each primary class has two subclasses (or types) of thick and thin fibrils, that is to say there are 4 different subclasses of fibrils in total. AFM images of these subclasses are shown in the Fig. 3. Thus, from now on, the following nomenclature will be used: the flexible thin fibrils will be marked as F1, the flexible thick fibrils as F2, the rigid thin fibrils as R1, and the rigid thick fibrils as R2. One should note that rigid thin fibrils (R1) still have larger diameters than flexible thick fibrils (F2).

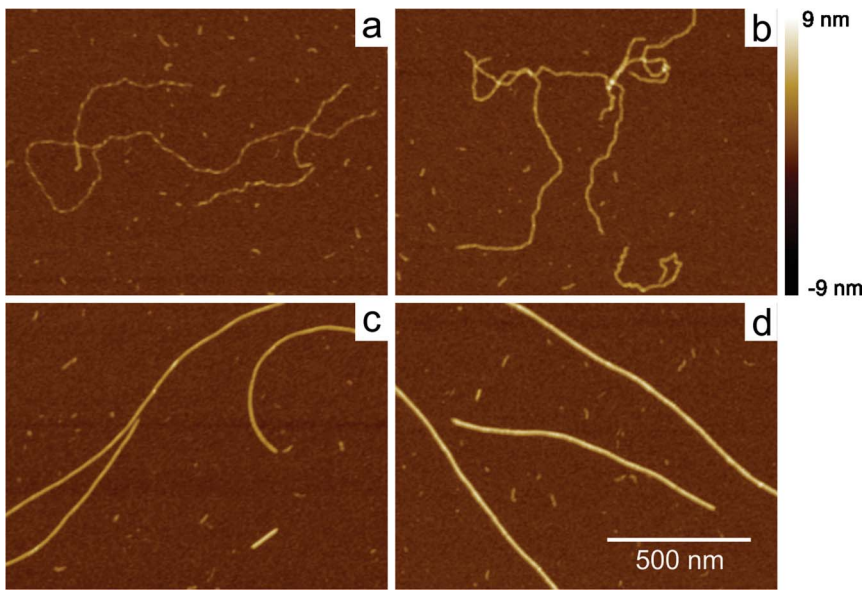

Fig. 3 AFM images of different subclasses of fibrils after 100 hours of incubation, (a) flexible thin (type F1), (b) flexible thick (type F2), (c) rigid thin (type R1), and (d) rigid thick (type R2). Scale bars apply to all images.

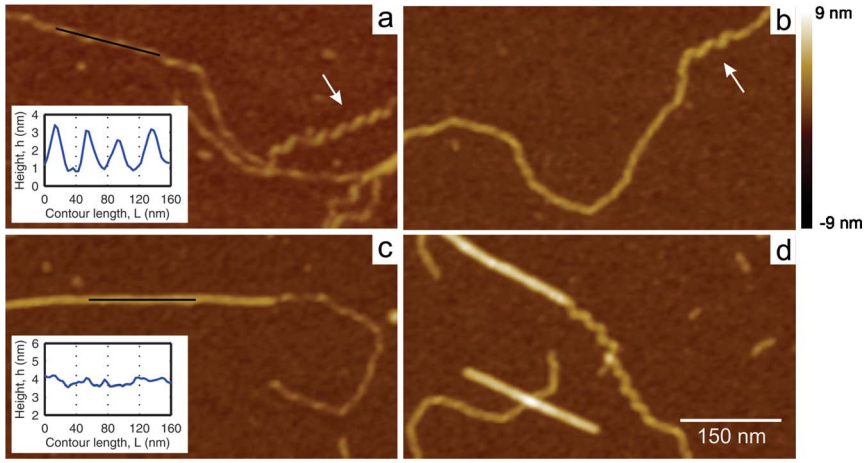

Fig. 4 High magnification AFM images of the BSA fibrils: (a) type F1, and (b) type F2. White arrows show areas where fibrils have left-handed helical ribbon conformation. Flexible left-handed ribbons are shown closing into rigid nanotubes in (c) F1 → R1 and (d) F2 → R2. Inset images show height profiles of F1 and R1 fibrils in longitudinal sections (black lines). Scale bars apply to all images.

A closer look at the BSA fibrils reveals very interesting results. The type F1 fibrils are generally well described from the structural morphology point of view by left-handed twisted ribbons with a quite regular periodicity of 40 ± 10 nm [Fig. 4(a), inset]. The type F2 fibrils also possess left-handedness with nonetheless irregular periodicity [Fig. 4(b)]. However, it is important to point out the occasional appearance of helical ribbon morphologies for both types of fibrils as can be observed in Fig. 4(a) and Fig. 4(b) where indicated by the white arrows. Although the fibrils are rather thin compared to the previously reported giant lysozyme and β-lactoglobulin helical ribbons,[35] they all share similar shapes. The coexistence of both polymorphic states, twisted and helical, within one fibril type indicates the possibility of a transformation between them. Such reorganization has already been observed in the supramolecular self-assembly of peptide amphiphiles,[68] bola amphiphiles,[69] and short modified Aβ(16–20) peptides.[70] Furthermore, a non-negligible fraction of rigid fibrils is contained at one end a part corresponding to a flexible fibril, as shown in Fig. 4(c, d): importantly, R1 fibrils have only F1 at their ends, while R2 fibrils have only F2 ends. Since no handedness or periodicity can be resolved along the rigid fibrils (see for example, the longitudinal profile for a representative R1 fibril shown in Fig. 4(c), inset), all these observations together suggest a closed cylindrical or tubular shape for the rigid fibrils. Similar images of helical ribbon progression into nanotubes, but at larger length scales was shown for enantiomeric-depsipeptide derivatives of the amyloidogenic peptide amylin(20–29).[71] These observations further support the idea that the fibrillation of BSA under these specific conditions proceeds as for short amyloidogenic peptides, *via* the transient state of a twisted ribbon to a helical ribbon to a nanotube.[70]

To perform statistical analysis we acquired the coordinates of over 4000 fibrils from several AFM images using special in-house software written for this purpose. Each traced object in the program is represented as a sequence of points that are connected with straight segments (contours). The typical step between the points is about the size of one pixel of an AFM image. Thus, each contour has a set of *XY*

(in the image plane) and Z (height) coordinates of all the points it incorporates. The contour can be deformed and fitted to a bright ridge of any elongated fibril in an image in order to follow accurately and precisely its middle line (see Methods section for details).

The coordinates of flexible fibrils (types F1 and F2) were obtained from high-resolution images of the 40 hours sample, while rigid fibrils (types R1 and R2) were separated from flexible fibrils during coordinate acquisition and tracked on images of the sample after 100 hours of incubation. No distinction between subclasses F1 and F2, as well as R1 and R2 were made during tracing. Hence, there were preliminarily only two data sets in total. The statistical investigation of Z coordinates is shown in Fig. 5, where left [Fig. 5(a, c)] and right [Fig. 5(b, d)] columns correspond to the analysis of flexible and rigid ensembles of fibrils, respectively. For convenience, subclasses of thin fibrils (F1 and R1) are represented by violet histogram bins, while subclasses of thick fibrils (F2 and R2) are depicted by blue-coloured bins. Fig. 5(a, b) display the fibrils' average height distributions. Two well-resolved peaks can be identified in both cases, separated by a minimum. The lowest frequency value between the peaks, *i.e.* the minimum, can be used to partition the tracked data in separate data sets corresponding to the thin and thick subclasses. The average heights at which this minimum occurs correspond to 3 nm for subclasses F1 and F2 [Fig. 5(a)] and 5.5 nm for subclasses R1 and R2 [Fig. 5(b)]. Fig. 5(c, d) illustrates overlapped histograms of all height values along all fibrils within a certain subgroup (each point of a contour gives one histogram count). Here are a few observations worth a short discussion. Due to a visible variation in height along the midline of the subclass F1 fibrils [Fig. 3(a) and Fig. 4(a, c)] the corresponding peak in Fig. 5(c) is much broader than the one in Fig. 5(a). All other peaks (F2, R1, and R2) in Fig. 5(c, d) have shapes close to

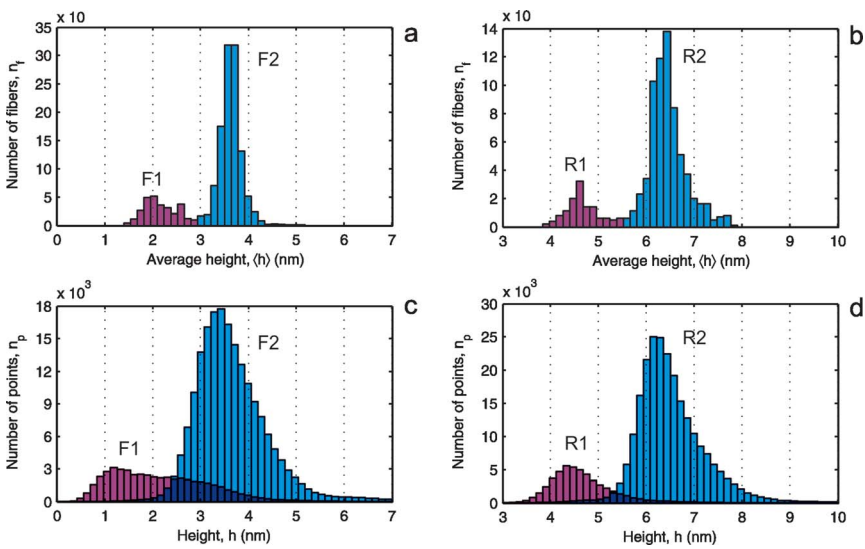

Fig. 5 Statistical analysis of the fibrils' Z coordinates. Average height value histograms for (a) flexible and (b) rigid classes. Blue and violet colours represent thick and thin fibrils, respectively. The minima separating the two sets of thin and thick fibrils are located at 3 nm for F1 and F2 (panel a), and 5.5 nm for R1 and R2 (panel b); (c–d) overlapped height histograms of all points belonging to flexible (c) and rigid (d) fibrils.

expected Gaussians, but curiously fat-tailed at the right sides. We believe that the source of the additional counts is the area along the contours in proximity to the intersection points of the crossing fibrils. As a result, in each case the height values having the highest frequencies are shifted to the left with respect to the peaks in the average height histograms. At the same time, these distributions define the average thickness of the fibrils in a more accurate way, removing the error coming from overlapped fibrils. Following this analysis, the mean fibril thicknesses $\langle h \rangle$ of the four subclasses are 2 nm for F1, 3.4 nm for F2, 4.4 nm for R1, and 6.3 nm for R2.

There are certain measurements in biology whose logarithms tend to have a normal distribution, for instance the lengths of inert appendages (hair, claws, nails, teeth), or quantitative values of living tissues (skin area, weight).[72] In this way, the measurements themselves have a log-normal distribution. If we assume that lengths of the BSA fibrils possess the same model behaviour, their histograms should fit to the following probability density function f(L):[73]

$$\mathrm{f}(L) = \frac{A}{L\sigma\sqrt{2\pi}} \mathrm{e}^{-\frac{(\ln(L)-\mu)^2}{2\sigma^2}}, \quad (1)$$

where L is the contour length of the fibrils, μ and σ are the mean value and the standard deviation of the length's natural logarithm, respectively, and A is a normalizing constant. Fig. 6(a, b) illustrates the fits for the length histograms of all fibril types, while the best-fit parameters are shown in Table 1. There is a good agreement between experimental data and the log-normal model behaviour with relatively high fit confidence (R^2_{adj}). As can be seen, both subclasses of flexible (F1 and F2), as well as rigid (R1 and R2) fibrils have very close μ and σ values, which is an indication of similar nucleation and growth rates. Moreover, as can be seen the

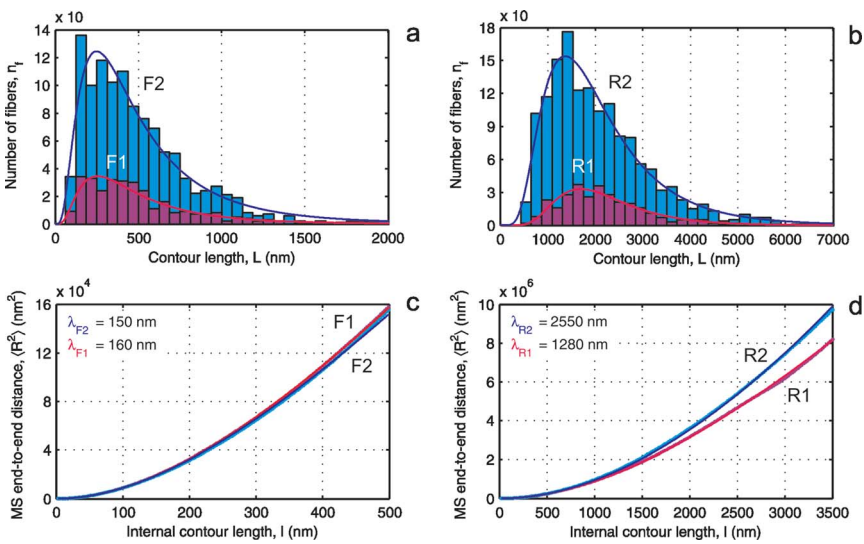

Fig. 6 Statistical analysis of the fibrils' *XY* coordinates. Contour length distributions for (a) flexible and (b) rigid classes. Blue and violet colours represent thick and thin fibrils respectively. Lines are fits with the log-normal distribution function (eqn 1); (c, d) mean squared end-to-end distance *versus* contour length fitted by eqn 4 to yield the persistence length.

Table 1 Statistical data and fitting parameters for the length distributions (N denotes the number of processed fibrils and L_{sum} is the sum of the fibril lengths)

Fibril type	N	L_{sum}, μm	μ	σ	A ($\times 10^3$)	R^2_{adj}
F1 (flexible thin)	296	147	6.04 ± 0.09	0.70 ± 0.07	19.8 ± 2.0	0.9319
F2 (flexible thick)	1133	552	6.04 ± 0.07	0.72 ± 0.06	73 ± 6	0.9535
R1 (rigid thin)	303	654	7.63 ± 0.05	0.44 ± 0.05	67 ± 7	0.9296
R2 (rigid thick)	1505	3295	7.51 ± 0.04	0.54 ± 0.04	329 ± 21	0.9712

Table 2 Summary of statistical evaluation for the BSA fibrils

Fibril type	$\langle h \rangle$, nm	$E[L]$, nm	$\langle L \rangle$, nm	Number ratio	Length ratio	λ, nm
F1 (flexible thin)	2.0 ± 0.2	~540	497	$N_{F1} : N_{F2}$	$L^{F1}_{sum} : L^{F2}_{sum}$	~160
F2 (flexible thick)	3.4 ± 0.2	~540	487	20.7 : 79.3	21.0 : 79.0	~150
R1 (rigid thin)	4.4 ± 0.2	~2270	2158	$N_{R1} : N_{R2}$	$L^{R1}_{sum} : L^{R2}_{sum}$	~1280
R2 (rigid thick)	6.3 ± 0.2	~2110	2189	16.8 : 83.2	16.6 : 83.4	~2550

total number ratios between two subclasses of flexible fibrils at 40 hours ($N_{F1} : N_{F2}$) and two subclasses of rigid fibrils at 100 hours ($N_{R1} : N_{R2}$) are roughly equal to 1/4 and 1/5, respectively (Table 2). The same values can be obtained for the total length ratios $L^{F1}_{sum} : L^{F2}_{sum}$ and $L^{R1}_{sum} : L^{R2}_{sum}$, since the μ and σ parameters are close to each other within one major class. This statistical result indicates that the conversion rate of the polymorphic transformation F1 → R1 is lower than F2 → R2.

If the fibril contour length L is a log-normally distributed variable, then its expected value $E[L]$ can be calculated according to the formula:[73]

$$E[L] = e^{\mu + \frac{\sigma^2}{2}}, \tag{2}$$

which defines the mean contour length predicted by the log-normal distribution. This can be directly compared with the arithmetic average contour length:

$$\langle L \rangle = \frac{L_{sum}}{N}. \tag{3}$$

Averages obtained from these equations for all subclasses are given in Table 2. They are found to be in good agreement, which again confirms that the log-normal distribution is a robust model to interpret the experimental fibril contour length spread.

The persistence length is a primary mechanical property of a polymer quantifying its bending propensity and is formally defined as the length over which angular correlations in the tangent direction are lost.[74] Here we use the internal mean squared end-to-end distance *versus* the internal contour length relationship for worm-like chain (WLC) model in 2D *via* the following equation:[75]

$$\langle R^2 \rangle = 4\lambda \left[l - 2\lambda \left(l - e^{-\frac{l}{2\lambda}} \right) \right], \tag{4}$$

where R is the direct distance between any pair of points on a fibril midline, l is the corresponding internal contour length, and λ is the persistence length.

Fig. 6(c, d) shows the fitting of experimental values for each subclass using eqn 4 ($R^2_{adj} > 0.99$ in all cases), and the extracted persistence length as the only fitting parameter. Interestingly, both types of flexible fibrils (thin and thick) have similar bendability with 160 nm and 150 nm persistence lengths, while rigid thick and thin fibrils have persistence lengths of 2550 nm and 1280 nm, respectively. The results obtained from the statistical analysis are combined in Table 2.

4. Conclusions

In this study we have investigated the fibrillation process of the globular protein BSA under high temperature (90 °C), acidic environment (pH 2) and long incubation times. BSA self-assembles into flexible left-handed twisted ribbons that can further transform into the helical ribbon polymorphic form and finally close into rigid nanotube-like structures. Accurate morphological analysis reveals a complex hierarchy of transient fibrils with four different types in total: flexible thin (F1), flexible thick (F2), rigid thin (R1), and rigid thick (R2). In order to characterise this polymorphism quantitatively, the main morphological parameters, *i.e.* contour length, average height, persistence length of the BSA fibrils, *etc.* were extracted in a statistical way. The analysis allowed us to conclude that for all subclasses of fibrils, the probability density function of finding a fibril of a given contour length follows a log-normal distribution and that rigid fibrils R1 and R2 originate from the closure of F1 and F2 fibrils, respectively.

Acknowledgements

The authors acknowledge support from the Swiss National Science Foundation: SNF (2-77002-11).

References

1 D. J. Selkoe, *Nature*, 2003, **426**, 900–904.
2 C. M. Dobson, *Nature*, 2003, **426**, 884–890.
3 F. Chiti and C. M. Dobson, *Annu. Rev. Biochem.*, 2006, **75**, 333–366.
4 F. Chiti and C. M. Dobson, *Nat. Chem. Biol.*, 2009, **5**, 15–22.
5 B. Caughey and P. T. Lansbury, *Annu. Rev. Neurosci.*, 2003, **26**, 267–298.
6 H. A. Lashuel and P. T. Lansbury Jr., *Q. Rev. Biophys.*, 2006, **39**, 167–201.
7 D. Eisenberg, R. Nelson, M. R. Sawaya, M. Balbirnie, S. Sambashivan, M. I. Ivanova, A. Ø. Madsen and C. Riekel, *Acc. Chem. Res.*, 2006, **39**, 568–575.
8 S. K. Maji, L. Wang, J. Greenwald and R. Riek, *FEBS Lett.*, 2009, **583**, 2610–2517.
9 D. Eisenberg and M. Jucker, *Cell*, 2012, **148**, 1188–1203.
10 F. G. Pearce, S. H. Mackintosh and J. A. Gerrard, *J. Agric. Food Chem.*, 2007, **55**, 318–322.
11 M. Lassé, J. A. Gerrard and F. G. Pearce, *Subcell Biochem.*, 2012, **65**, 253–270.
12 C. Veerman, L. M. C. Sagis and E. van der Linden, *Macromol. Biosci.*, 2003, **3**, 243–247.
13 A. Kroes-Nijboer, P. Venema and E. van der Linden, *Food Funct.*, 2012, **3**, 221–227.
14 R. Mezzenga, P. Schurtenberger, A. Burbidge and M. Michel, *Nat. Mater.*, 2005, **4**, 729–740.
15 T. Nicolai, M. Britten and C. Schmitt, *Food Hydrocolloids*, 2011, **25**, 1945–1962.
16 T. P. Knowles and M. J. Buehler, *Nat. Nanotechnol.*, 2011, **6**, 469–479.
17 S. G. Zhang, *Nat. Biotechnol.*, 2003, **21**, 1171–1178.
18 C. Li, J. Adamcik and R. Mezzenga, *Nat. Nanotechnol.*, 2012, **7**, 421–427.
19 I. Cherny and E. Gazit, *Angew. Chem., Int. Ed.*, 2008, **47**, 4062–4069.
20 S. L. Gras, *Adv. Chem. Eng.*, 2009, **35**, 161–209.
21 L. Adler-Abramovich, N. Kol, I. Yanai, D. Barlam, R. Z. Shneck, E. Gazit and I. Rousso, *Angew. Chem., Int. Ed.*, 2010, **49**, 9939–9942.
22 J. Adamcik and R. Mezzenga, *Macromolecules*, 2012, **45**, 1137–1150.

23 T. P. Knowles, A. W. Fitzpatrick, S. Meehan, H. R. Mott, M. Vendruscolo, C. M. Dobson and M. E. Welland, *Science*, 2007, **318**, 1900–1903.
24 C. Lara, I. Usov, J. Adamcik and R. Mezzenga, *Phys. Rev. Lett.*, 2011, **107**, 238101.
25 L. M. C. Sagis, C. Veerman and E. van der Linden, *Langmuir*, 2004, **20**, 924–927.
26 D. M. Ridgley and J. R. Barone, *ACS Nano*, 2013, **7**, 1006–1015.
27 C. Lara, S. Gourdin-Bertin, J. Adamcik, S. Bolisetty and R. Mezzenga, *Biomacromolecules*, 2012, **13**, 4213–4221.
28 C. Veerman, G. de Schiffart, L. M. Sagis and E. van der Linden, *Int. J. Biol. Macromol.*, 2003, **33**, 121–127.
29 S. G. Bolder, H. Hendrickx, L. M. C. Sagis and E. van der Linden, *J. Agric. Food Chem.*, 2006, **54**, 4229–4234.
30 J. M. Jung, G. Savin, M. Pouzot, C. Schmitt and R. Mezzenga, *Biomacromolecules*, 2008, **9**, 2477–2486.
31 S. Bolisetty, J. Adamcik and R. Mezzenga, *Soft Matter*, 2011, **7**, 493–499.
32 L. N. Arnaudov and R. de Vries, *Biomacromolecules*, 2006, **7**, 3490–3498.
33 S. M. Loveday, X. L. Wang, M. A. Rao, S. G. Anema and H. Singh, *J. Agric. Food Chem.*, 2011, **59**, 8467–8474.
34 S. M. Loveday, J. Su, M. A. Rao, S. G. Anema and H. Singh, *J. Agric. Food Chem.*, 2012, **60**, 5229–5236.
35 C. Lara, J. Adamcik, S. Jordens and R. Mezzenga, *Biomacromolecules*, 2011, **12**, 1868–1875.
36 S. M. Loveday, M. A. Rao, L. K. Creamer and H. Singh, *J. Food Sci.*, 2009, **74**, R47–55.
37 E. Frare, P. Polverino De Laureto, J. Zurdo, C. M. Dobson and A. Fontana, *J. Mol. Biol.*, 2004, **340**, 1153–1165.
38 L. N. Arnaudov and R. de Vries, *Biophys. J.*, 2005, **88**, 515–526.
39 K. Sasahara, H. Yagi, H. Naiki and Y. Goto, *J. Mol. Biol.*, 2007, **372**, 981–991.
40 J. Goers, S. E. Permyakov, E. A. Permyakov, V. N. Uversky and A. L. Fink, *Biochemistry*, 2002, **41**, 12546–12551.
41 R. M. C. Dawson, D. C. Elliott, W. H. Elliott and K. M. Jones, Data for biochemical research, 1986.
42 D. Bulone, V. Martorana and L. S. P. Biagio, *Biophys. Chem.*, 2001, **91**, 61–69.
43 N. K. Holm, S. K. Jespersen, L. V. Thomassen, T. Y. Wolff, P. Sehgal, L. A. Thomsen, G. Christiansen, C. B. Andersen, A. D. Knudsen and D. E. Otzen, *Biochim. Biophys. Acta, Proteins Proteomics*, 2007, **1774**, 1128–1138.
44 V. Vetri, F. Librizzi, M. Leone and V. Militello, *Eur. Biophys. J.*, 2007, **36**, 717–725.
45 E. Bramanti, C. Ferrari, V. Angeli, M. Onor and R. E. Synovec, *Talanta*, 2011, **85**, 2553–2561.
46 C. Veerman, L. M. C. Sagis, J. Heck and E. van der Linden, *Int. J. Biol. Macromol.*, 2003, **31**, 139–146.
47 K. Murayama and M. Tomida, *Biochemistry*, 2004, **43**, 11526–11532.
48 M. Murata, F. Tani, T. Higasa, N. Kitabatake and E. Doi, *Biosci., Biotechnol., Biochem.*, 1993, **57**, 43–46.
49 M. Bhattacharya, N. Jain and S. Mukhopadhyay, *J. Phys. Chem. B*, 2011, **115**, 4195–4205.
50 R. Su, W. Qi, Z. He, Y. Zhang and F. Jin, *Food Hydrocolloids*, 2008, **22**, 995–1005.
51 S. M. Vaiana, A. Emanuele, M. B. Palma-Vittorelli and M. U. Palma, *Proteins: Struct., Funct., Bioinf.*, 2004, **55**, 1053–1062.
52 V. Militello, C. Casarino, A. Emanuele, A. Giostra, F. Pullara and M. Leone, *Biophys. Chem.*, 2004, **107**, 175–187.
53 V. Vetri, M. D'Amico, V. Foderà, M. Leone, A. Ponzoni, G. Sberveglieri and V. Militello, *Arch. Biochem. Biophys.*, 2011, **508**, 13–24.
54 M. J. W. Povey, J. D. Moore, J. Braybrook, H. Simons, R. Belchamber, M. Raganathan and V. Pinfield, *Food Hydrocolloids*, 2011, **25**, 1233–1241.
55 J. Adamcik and R. Mezzenga, *Curr. Opin. Colloid Interface Sci.*, 2012, **17**, 369–376.
56 J. Adamcik, J.-M. Jung, J. Flakowski, P. D. L. Rios, G. Dietler and R. Mezzenga, *Nat. Nanotechnol.*, 2010, **5**, 423–428.
57 T. P. Knowles, A. W. Fitzpatrick, S. Meehan, H. R. Mott, M. Vendruscolo, C. M. Dobson and M. E. Welland, *Science*, 2007, **318**, 1900–1903.
58 A. Relini, S. Torrassa, R. Ferrando, R. Rolandi, S. Campioni, F. Chiti and A. Gliozzi, *Biophys. J.*, 2010, **98**, 1277–1284.
59 J. F. Smith, T. P. Knowles, C. M. Dobson, C. E. Macphee and M. E. Welland, *Proc. Natl. Acad. Sci. U. S. A.*, 2006, **103**, 15806–15811.
60 J. Adamcik, A. Berquand and R. Mezzenga, *Appl. Phys. Lett.*, 2011, **98**, 193701.
61 J. Adamcik, C. Lara, I. Usov, J. S. Jeong, F. S. Ruggeri, G. Dietler, H. A. Lashuel, I. W. Hamleyd and R. Mezzenga, *Nanoscale*, 2012, **4**, 4426–4429.
62 K. Sweers, K. van der Werf, M. Bennink and V. Subramaniam, *Nanoscale Res. Lett.*, 2011, **6**, 270.

63 I. Usov, R. Mezzenga, submitted.
64 M. B. Smith, H. Li, T. Shen, X. Huang, E. Yusuf and D. Vavylonis, *Cytoskeleton*, 2010, **67**, 693–705.
65 M. Kass, A. Witkin and D. Terzopoulos, *Int. J. Comput. Vision*, 1988, 321–331.
66 P. E. Hart, N. J. Nilsson and B. A. Raphael, *IEEE Trans. Syst. Sci. Cybern.*, 1968, **SSC-4**(2), 100–107.
67 S. Jordens, J. Adamcik, I. Amar-Yuli and R. Mezzenga, *Biomacromolecules*, 2011, **12**, 187–193.
68 E. T. Pashuck and S. I. Stupp, *J. Am. Chem. Soc.*, 2010, **132**, 8819–8821.
69 L. Ziserman, H. Y. Lee, S. R. Raghavan, A. Mor and D. Danino, *J. Am. Chem. Soc.*, 2011, **133**, 2511–2517.
70 J. Adamcik, V. Castelletto, S. Bolisetty, I. W. Hamley and R. Mezzenga, *Angew. Chem., Int. Ed.*, 2011, **50**, 5495–5498.
71 R. C. Elgersmaa, G. E. Mulder, G. Posthuma, D. T. S. Rijkers and R. M. J. Liskamp, *Tetrahedron Lett.*, 2008, **49**, 987–991.
72 J. S. Huxley and F. B. Churchill, in *Problems of Relative Growth*, Johns Hopkins University Press, 1993.
73 A. M. Mood, F. A. Graybill and D. C. Boes, in *Introduction to the Theory of Statistics*, McGraw-Hill, 1973.
74 P. J. Flory, in *Statistical Mechanics of Chain Molecules*, Hanser Gardner Publications, 1989.
75 C. Rivetti, M. Guthold and C. Bustamante, *J. Mol. Biol.*, 1996, **264**, 919–932.

